Application of Time-Resolved Step-Scan Fourier Transform Infrared Spectroscopy to Photochemical Mechanistic Investigations of Alkyl Phenylglyoxylates[†,‡]

A. V. Fedorov, E. O. Danilov, A. G. Merzlikine, M. A. J. Rodgers,* and D. C. Neckers*

Center for Photochemical Sciences, Bowling Green State University, Bowling Green, Ohio 43403

Received: July 9, 2002; In Final Form: October 30, 2002

The photochemical reactivity of alkyl phenylglyoxylates has been investigated using time-resolved step-scan Fourier transform infrared spectroscopy. The time-resolved FTIR spectra of hexane solutions of methyl (MPG), ethyl (EPG), and isopropyl (iPPG) phenylglyoxylates and benzene solutions of MPG display two major transient absorption peaks in the carbonyl fundamental region around 1661 and 2105 cm^{-1}. On the basis of the spectroscopic and kinetic evidence, the 1661 cm^{-1} transitions are assigned to the carbonyl fundamental of the triplet state of the corresponding alkyl phenylglyoxylate. The 2105 cm^{-1} band is attributed to the carbonyl stretch of α-hydroxyphenyl ketene, which is the postulated intermediate of the intramolecular hydrogen abstraction in alkyl phenylglyoxylates. These assignments are supported by the results of DFT calculations. From kinetic time profiles for the two observed transient infrared bands, the rate constants for the intra- and intermolecular γ-hydrogen abstraction were obtained and compared for methyl, ethyl, and isopropyl phenylglyoxylates. The reasons for the difference between the rate constants for glyoxylates and aromatic ketones are discussed.

Introduction

Time-resolved infrared (TR IR) spectroscopy in the nanosecond time domain is a powerful technique, which compliments conventional UV−vis laser flash-photolysis (LFP). This method becomes especially useful in cases where the absence of a UV chromophore or a low extinction coefficient of the UV absorption prevents the use of LFP. In addition, IR bands are more structure-specific than UV−vis transitions. Experimental methods of TR IR spectroscopy can be either step-scan Fourier transform or dispersive. The former was extensively used to study the MLCT excited states of the transition metal complexes,[1] transformations in biomolecules,[2] and behavior of short-lived species in zeolites and other solid-state matrixes,[3] while the latter explores organic transients such as various radicals,[4] carbenes,[5] and metastable species including ketenes.[6] With few exceptions,[7] the step-scan method was not often applied to study the organic systems in solution. Here we report the use of the time-resolved step-scan FTIR spectroscopy to investigate the photochemistry of alkyl phenylglyoxylates.

Alkyl phenylglyoxylates (APGs) are used as photoinitiators in the polymerization of urethane acrylates, and have potential applications for laser induced surface processes. The photoexcitation of APGs results in both inter- and intramolecular hydrogen abstraction (Scheme 1).[8−10]

The intermolecular hydrogen abstraction dominates at [APG] greater than 0.1 M producing the relatively long-lived mandelate and other radicals.[9] At [APG] lower than 10^{-1} M, intramolecular γ−hydrogen abstraction prevails yielding a short-lived (∼16 ns[11]) 1,4-biradical (**2**). Biradical cleavage results in formation of the α-hydroxyphenyl ketene (**3**) and a carbonyl product. In the later stages of the reaction, the intermediate ketene is proposed to undergo photodecarbonylation followed by rearrangement of the carbene produced into benzaldehyde. The formation of **3** has been widely accepted since it was first proposed[8] on the basis of the analysis of photolysis products[8−10] and indirectly confirmed by time-resolved UV LFP studies.[12] In a previous communication,[13] we reported direct observation and characterization of the α-hydroxyphenyl ketene **3** by time-resolved step-scan Fourier transform infrared spectroscopy with emphasis on the spectroscopic evidence. The present work outlines more detailed studies of alkyl phenylglyoxylates with the focus on both spectroscopic and kinetic information obtained from the TR FTIR spectra.

Experimental Section

Time-Resolved FTIR Spectrometer. The major components of the step-scan TR FTIR spectrometer are Spectra Physics GCR series pulsed YAG:Nd^{3+} laser, Bruker model IFS55 FTIR spectrometer, fast electronics for signal processing, Tektronix TDS 3032 digital phosphor oscilloscope, and Spectrum PAD82a computer ADC board for data visualization and acquisition (Figure 1). Experimental synchronization of the laser excitation pulse and interferometer data acquisition was controlled by Stanford Research System (model DG 535) timing generator. Two channels were used to fire the laser flashlamps and the Q-switch and another channel was used to trigger the transient digitizer and oscilloscope.

Third harmonic of the YAG:Nd^{3+} laser (354.7 nm) operating at 10 Hz repetition rate was used in the experiments. The laser pulse duration was ∼7 ns with the energy up to 40 mJ/pulse. The laser excitation beam (∼10 mm in diameter) was directed through an iris aperture (6 mm in diameter) and then overlapped with the infrared beam in the sample cell within the sample compartment of the FTIR spectrometer. The laser beam energy

[†] Part of the special issue "George S. Hammond & Michael Kasha Festschrift". Dedicated in honor of George S. Hammond, whose brilliant insights are the basis for this work, on the occasion of his 81st birthday. Also in honor of Prof. Dr. J. W. Neckers, on the occasion of his 101st birthday and 80th year in science.

[‡] Center for Photochemical Sciences Contribution #487.

10.1021/jp021573w CCC: $25.00
Published on Web 02/07/2003

SCHEME 1

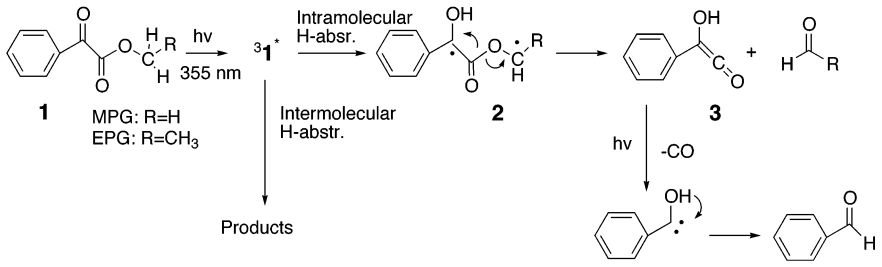

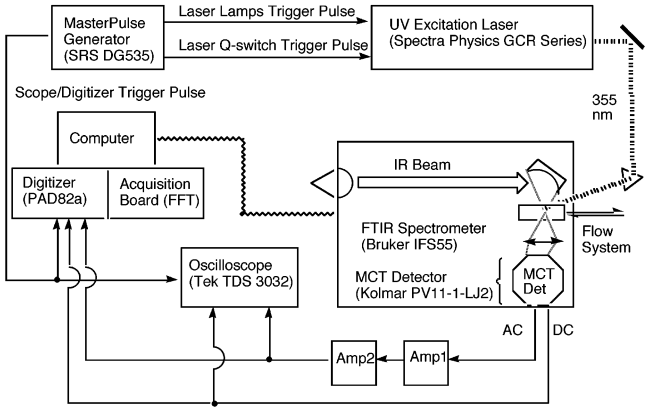

Figure 1. Schematic representation of the experimental setup.

after the aperture was 10 mJ per pulse. A 1 mm path length flow cell with CaF_2 windows was used for the measurements. After passing the sample, the divergent infrared beam was recollimated and focused onto Kolmar Technologies model PV11-1-LJ2 liquid-N_2-cooled photovoltaic MCT detector equipped with a fast internal preamplifier.

The spectrometer was mounted on a vibrationally proof optical table and operated in the step-scan mode. A globar IR source and KBr beam splitter were used for the mid-IR measurements. To limit the number of interferogram points and the acquisition time, the infrared range was limited to 1350−2350 cm^{-1} by a combination of longwave-pass and shortwave-pass filters (Spectrogon). In step-scan FTIR measurements, intensities of the mid-IR time-dependent difference spectra are much smaller than are the intensities of the static spectra. To measure these signals with high sensitivity, an AC-coupled IR detector output with further signal amplification was required. Because the resulting difference spectra may contain both positive and negative peaks, the standard Metz and Forman phase correction algorithm is not applicable in this case. In particular, the negative intensities may be misinterpreted as positive intensities with a certain phase shift.[14] To extract reliable phase information, a separate DC-coupled interferogram was acquired simultaneously with the AC-coupled signal. The AC signal from the internal preamplifier of the detector was fed into external amplifiers (EG&G ORTECH model 535 Quad and Comlinear model 103) with the total gain of about 200 and then simultaneously into channel A of the PAD82a transient digitizer board and oscilloscope channel 1. The DC signal was directed onto channel B of the PAD82a and oscilloscope channel 2. The oscilloscope was used to ensure that the signals did not exceed the ±1 V dynamic range of the digitizer.

The electronic circuit was examined to ensure it was not restricting the bandwidth within the temporal range of interest. The band-pass of the amplification circuit was broad enough to accommodate the signals between ∼4 ns and ∼10 ms. The overall band-pass was limited by the 30 ns MCT detector response time on the high-frequency side and 1 ms fall off due to the internal MCT preamplifier on the low-frequency side.

The acquisition time for the single TR FTIR spectrum with 4 cm^{-1} resolution was typically 25−35 min. After collecting the spectrum, the data was converted into the DataTable format using internal Bruker OPUS MACRO routine and a custom written TRACER software. The data were further processed by the Microcal Origin or Sigma Plot.

Due to restrictions of the PAD82a transient recorder (one can only store single channel data rather than an absorbance or transmittance spectrum) and because the PAD82a digitizer handles data in arbitrary units, conversion to ΔA was required. The time-resolved IR absorption spectrum was obtained by converting the arbitrary digitizer units into the difference spectrum: $\Delta A = -\log(1 + \Delta S/S)$ where ΔS is the difference IR spectrum with UV excitation "on" and S is the static spectrum of the sample with the UV laser "off".

Test of the Spectrometer. To test the operational capabilities of the TR FTIR system, the behavior of the benzoyl radical obtained from the 355 nm photolysis of 2,2-dimethylpropiophenone (DMPP) was investigated. In accord with previous dispersive TR IR spectroscopic measurements,[4a,b] the carbonyl band of this radical was observed at 1828 cm^{-1}, which is significantly blue shifted relative to the C═O absorption band of DMPP at 1685 cm^{-1}. The benzoyl radical absorption decayed within a few microseconds with predominantly second-order kinetics resulting from radical−radical recombination. The decay rate of the benzoyl radical can be increased by the addition of a radical quencher such as CCl_3Br. In this case, the second band at 1780 cm^{-1} corresponding to the C═O stretch of benzoyl bromide appears as transition at 1828 cm^{-1} disappears. In contrast to the previous investigations,[4a,b] the present experiments were conducted with higher concentrations of DMPP (10−40 mM). The lifetime of the benzoyl radicals was dependent on the concentration of DMPP pointing to interactions of the benzoyl radicals with a second DMPP molecule. The linear plot of k_{obs} vs [DMPP] yields the quenching constant (k_{sq}) of 7.2×10^6 $M^{-1}\cdot s^{-1}$. A quenching constant of 4.1×10^8 $M^{-1}\cdot s^{-1}$ was obtained with addition of CCl_3Br. This is close to the 2.2×10^8 $M^{-1}\cdot s^{-1}$ value reported previously.[4a,b]

Time-Resolved UV−Vis Laser Flash Photolysis. Nanosecond UV−vis LFP studies were conducted using the setup previously described.[9] Samples were irradiated in the 1 cm cuvette and Ar was continuously purged through the solution during the experiments.

Calculations. Optimized geometries and IR frequencies for all molecules of interest were calculated using Gaussian98[14] with B3LYP/6-31+G(d) level of theory. All calculated frequencies were scaled by a factor of 0.96, which is typical for this level of theory.[15]

Materials. Methyl phenylglyoxylate (MPG) and ethyl phenylglyoxylate (EPG) were purchased from Aldrich and used without further purification. Isopropyl phenylglyoxylate (iPPG)

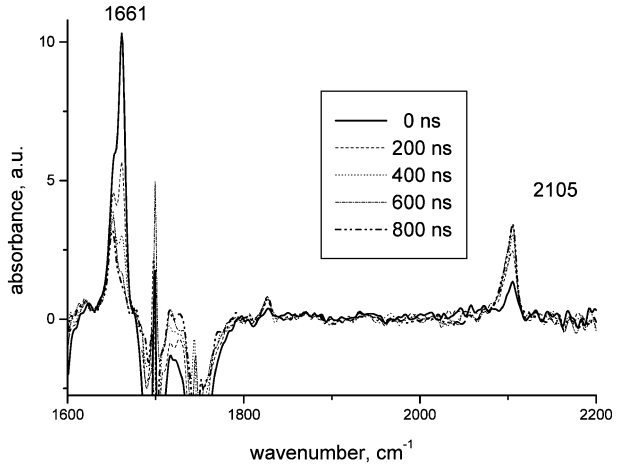

Figure 2. Infrared transient absorption spectra of 40 mM Ar-saturated hexane solution of MPG following the 355 nm laser excitation. Spectra displayed each 200 ns in the 0−1000 ns time interval. Two absorption peaks are centered at 1661 and 2105 cm^{-1}.

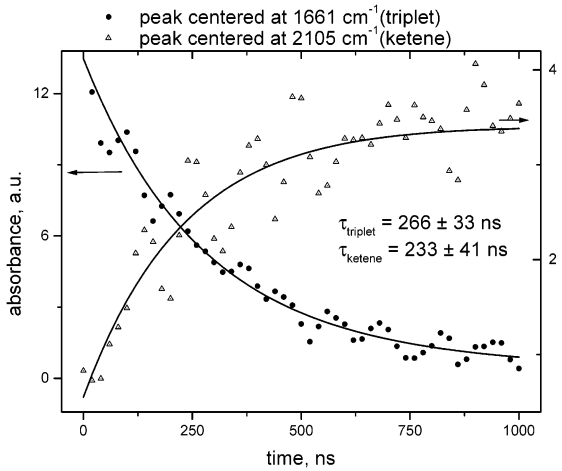

Figure 3. Kinetic traces observed at 1661 and 2105 cm^{-1} in MPG solution. Dots represent experimental data; lines are calculated best fits to a biexponential function (fast components used).

and *tert*-butyl phenylglyoxylate (TBPG) were synthesized according to the previously outlined procedure.[9] The purity of each glyoxylate was verified by NMR and GC/MS. Spectrophotometric grade solvents were used, and 1500−2300 cm^{-1} (hexane) and 1500−1800, 1850−1950, 2000−2500 cm^{-1} (benzene) spectroscopic windows were accessible for the TR IR measurements.

Results and Discussion

The FTIR spectra displayed each 200 ns in the time interval from 0 to 1000 ns after the 355 nm excitation of 40 mM hexane solution of MPG are shown in Figure 2. Clearly, two transient absorptions can be identified. The band at 1661 cm^{-1} rises sharply and decays within a few microseconds while the second transition at 2105 cm^{-1} grows in at the same time. The decay and growth of the corresponding kinetic profiles (Figure 3) are concomitant suggesting that the transient absorbing at 2105 cm^{-1} derives from the 1661 cm^{-1} species.

A similar spectral situation was observed in benzene. At 16 cm^{-1} resolution, the transitions practically unshifted around 1661 and 2105 cm^{-1} dominate the spectrum. Kinetic profiles are concomitant (lifetimes are around 500 ns) but lifetimes are longer in benzene than in hexane.

The IR spectrum does not change dramatically when hexane solutions of EPG are examined (Figure 4). The kinetic profiles

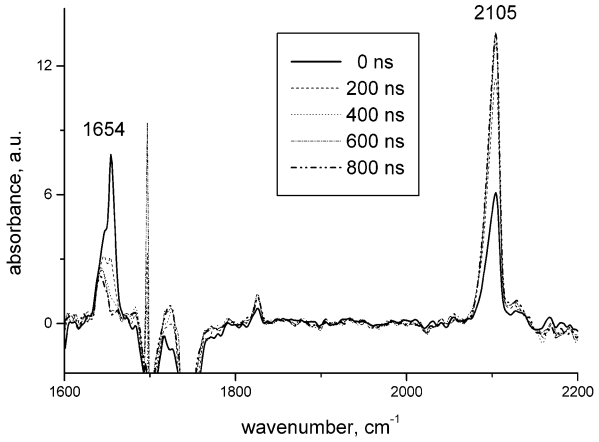

Figure 4. Infrared transient absorption spectra of 40 mM Ar-saturated hexane solution of EPG following the 355 nm laser excitation. Spectra displayed each 200 ns in the 0−1000 ns time interval. Two absorption peaks are observed at 1654 and 2105 cm^{-1}.

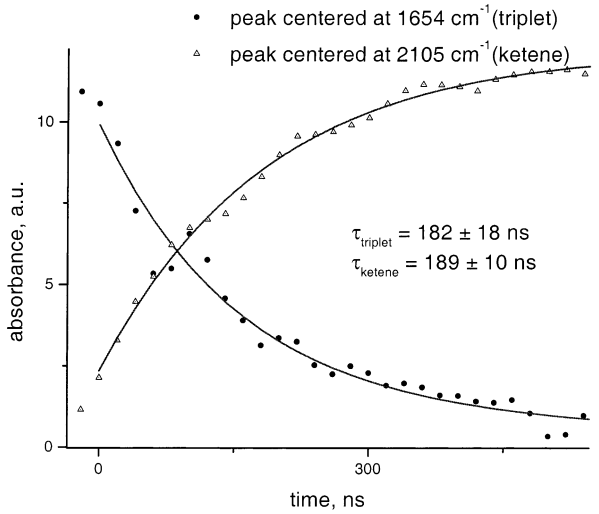

Figure 5. Kinetic traces observed at 1654 and 2105 cm^{-1} in EPG solution. Dots represent experimental data; lines are calculated best fits to a single-exponential function.

at 1654 and 2105 cm^{-1} remain concomitant, but with shorter lifetimes compared to the corresponding MPG values (Figure 5).

The spectral picture remains similar in the case of iPPG (Figure 6). The triplet decay rates are concomitant in the 10−30 mM concentration range. However, the triplet lifetime in the 40 mM solution is abnormally long.

Negative bands corresponding to the depletion of the starting glyoxylate are observed at 10 mM concentration (Figures 7−9). At 40 mM concentration, the IR spectrum of the starting glyoxylate is saturated in the carbonyl region (1699 and 1747 cm^{-1} for MPG) making the spectral interval within ±15 cm^{-1} of the these bands unsuitable for TR IR studies. This also prevents detection of any transients absorbing in these particular regions. This is similar to the effect of a solvent, which prevents the transient IR measurements in the regions of the solvent absorption bands.

In our earlier communication[13] we suggested the assignments for the two bands observed in the TR FTIR spectrum. The justification for these assignments is discussed here in a greater detail. The 2105 cm^{-1} band can be attributed to α-hydroxyphenyl ketene on the bases of the following arguments. First, the specific IR frequency of this band significantly narrows the list of potential candidates. Only a few functional groups display

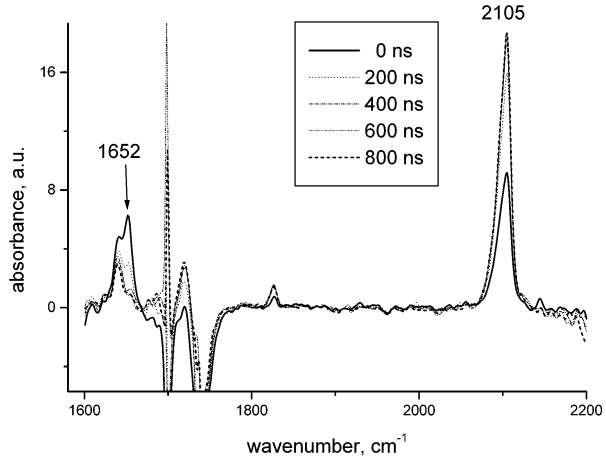

Figure 6. Infrared transient absorption spectra of 40 mM Ar saturated hexane solution of iPPG following the 355 nm laser excitation. Spectra displayed each 200 ns in the 0−1000 ns time interval. Two absorption peaks are observed at 1652 and 2105 cm^{-1}.

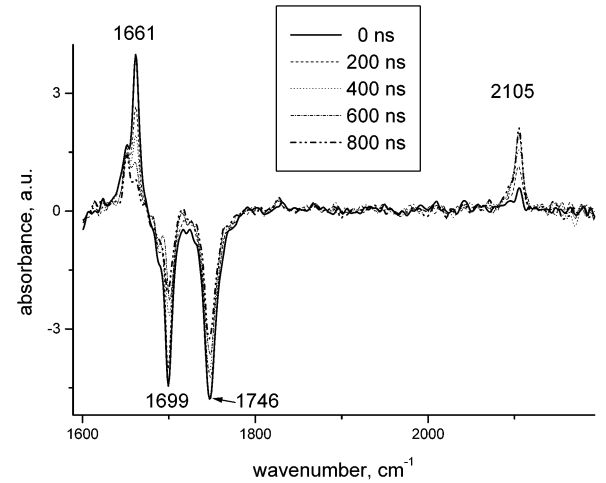

Figure 7. Infrared transient absorption spectra of 10 mM Ar-saturated hexane solution of MPG following the 355 nm laser excitation. Spectra displayed each 200 ns in the 0−1000 ns time interval. Two absorption peaks are observed at 1661 and 2105 cm^{-1}.

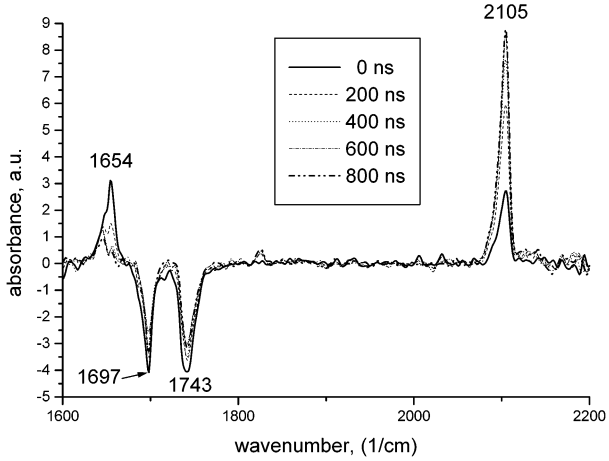

Figure 8. Infrared transient absorption spectra of 10 mM Ar-saturated hexane solution of EPG following the 355 nm laser excitation. Spectra displayed each 200 ns in the 0−1000 ns time interval. Two absorption peaks are observed at 1654 and 2105 cm^{-1}.

their mid-IR absorptions in the 2000−2500 cm^{-1} region (e.g., CC triple bonds or CN triple bonds).[17] This, for example, eliminates the α-lactone, a possible product of biradical cyclization. Ketenes, on the other hand, are known to display a

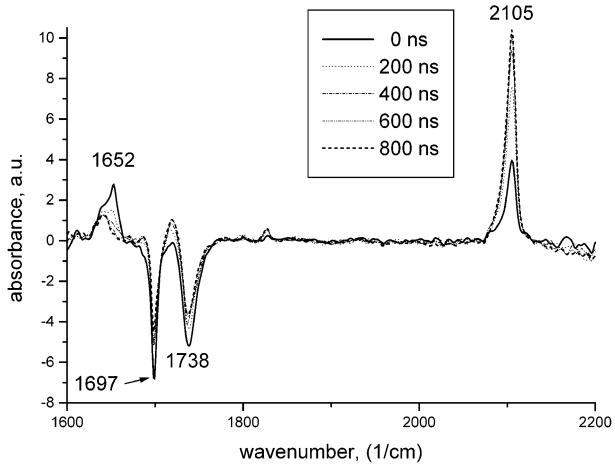

Figure 9. Infrared transient absorption spectra of 10 mM Ar-saturated hexane solution of iPPG following the 355 nm laser excitation. Spectra displayed each 200 ns in the 0−1000 ns time interval. Two absorption peaks are observed at 1652 and 2105 cm^{-1}.

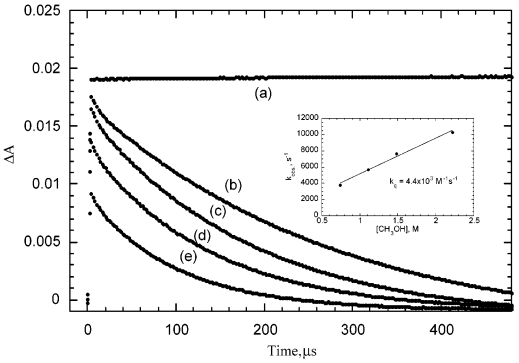

Figure 10. Kinetic traces observed at 2100 cm^{-1} for 40 mM Ar-saturated benzene solutions of MPG in the absence of methanol (a) and upon addition of 0.74 M (b), 1.11 M (c), 1.48 M (d) and 2.22 M (e) of methanol (16 cm^{-1} resolution). Inset: Quenching plot of k_{obs} vs methanol concentration. The slope of the straight line represents the quenching rate constant of α-hydroxyphenylketene by methanol.

characteristic absorption in the 2085−2197 cm^{-1} region due to the antisymmetric stretch of the C═C═O moiety.[6c,17,18]

Second, the long lifetime and specific interactions of the 2105 cm^{-1} species with quenchers provide further foundation for this assignment. The 2105 cm^{-1} signal does not decay for over 500 μs in the absence of the quencher. When 0.74−2.22 M of methanol was added to the MPG solution, the lifetime of the 2105 cm^{-1} band was shortened to hundreds of microseconds (Figure 10). The linear plot of k_{obs} vs [CH_3OH] (inset of Figure 10) yields the quenching rate constant of $4.4 \cdot 10^3$ $M^{-1} \cdot s^{-1}$. This value is close to the quenching rate constants with methanol obtained previously for other ketenes.[19]

The intensity of the ketene signal consistently decreases as the [CH_3OH] increases, which can be observed from the traces in Figure 10. This indicates that one of the ketene's precursors (APG triplet or biradical) reacts with methanol decreasing the ketene yield. The monitoring of the APG triplet lifetime in hexane solutions using UV flash-photolysis indicated that it is unaffected by the addition of methanol. This makes the interaction between biradical and methanol responsible for the observed decrease of the ketene signal.

Shortening of the 2105 cm^{-1} transient lifetime was also observed when the starting MPG solution was saturated with oxygen (Figure 11). The interactions with CH_3OH and oxygen are typical for ketenes.[18] These observations strongly argue

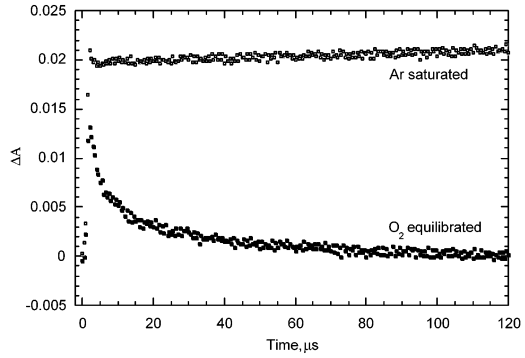

Figure 11. Time profiles observed for decay of 2100 cm^{-1} species in 40 mM Ar-saturated (a) and air O_2 equilibrated and (b) hexane solutions of MPG (16 cm^{-1} resolution).

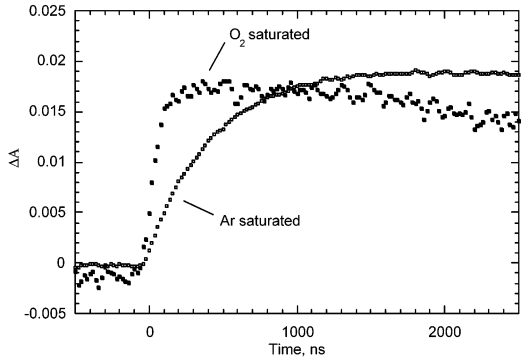

Figure 12. Time profiles observed for growth of intermediate at 2100 cm^{-1} in 40 mM Ar-saturated (a) and O_2 saturated and (b) benzene solutions of MPG (16 cm^{-1} resolution).

against the possibility of 2105 cm^{-1} species being carbon monoxide, which is one of the postulated products of ketene decarbonylation. In addition, the late appearance of CO in the photolysis mixture[8,9] is inconsistent with the concommitance of the kinetic traces.

Third, the experimental IR frequencies can be compared to the calculated IR frequencies predicted with a relatively high level of accuracy and reliability. The predicted C═C═O frequency of α-hydroxyphenyl ketene is 2096 cm^{-1}, which is close to 2105 cm^{-1} the experimental value.

Since it is a precursor for the 2105 cm^{-1} transition, the 1661 cm^{-1} band can be attributed to either glyoxylate triplet or biradical. The following information supports the assignment of 1661 cm^{-1} band to the glyoxylate triplet. First, the fast growth (within the 30 ns instrument response time) of the 1661 cm^{-1} species indicates that it originates from a short-lived singlet state of the alkyl phenylglyoxylate (APG) and that it can reasonably be attributed to the APG triplet. Second, this assignment can be confirmed by the introduction of the structural changes in glyoxylate. The intramolecular H-abstraction and, hence, the formation of both biradical and ketene can be eliminated, if all the γ-hydrogens in MPG, EPG or iPPG are replaced by methyl groups. In this case, only glyoxylate triplet absorption would remain in the spectrum because the alteration of glyoxylate aliphatic tail is not expected to significantly change the frequency of the carbonyl fundamental. The TR FTIR spectrum of the resulting *tert*-butyl phenylglyoxylate (TBPG) in hexane displays single transient absorption at 1643 cm^{-1} with the 1004 ns lifetime (Figure 12). This confirms the assignment of the 1661 cm^{-1} transition to the glyoxylate triplet and not to the biradical. Third, both the lifetime of 1661 and the rise time of 2105 cm^{-1} species decrease dramatically (72 ± 20 and 75 ± 5 ns, respectively) when the starting solution is saturated with

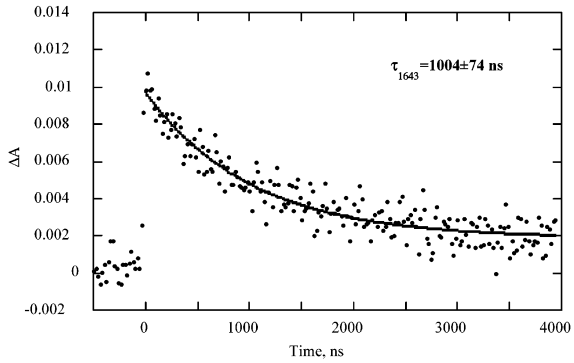

Figure 13. Kinetic trace observed at 1643 cm^{-1} following the 355 nm laser excitation of TBPG (40 mM) in Ar-saturated hexane. Dots represent experimental data, line is calculated best fit to a single-exponential function.

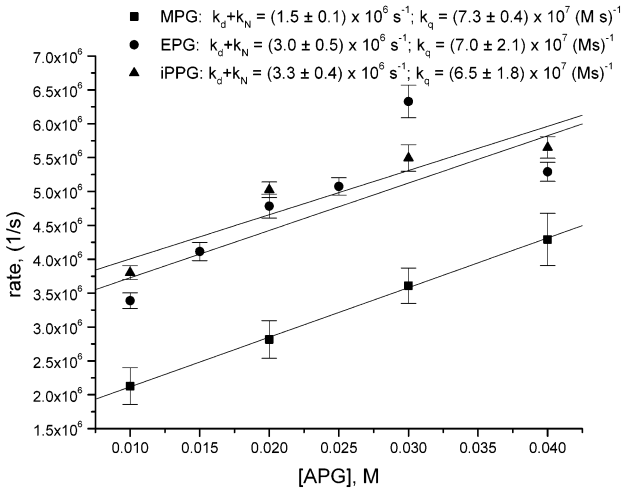

Figure 14. Typical quenching plots ($1/\tau_{obs} = k_{obs}$ vs [APG]) obtained for hexane solutions of MPG (circles), EPG (triangles), and iPPG (squares). The shown data is obtained from the rise time of ketene at 2100 cm^{-1}. The slope of the straight line is the intermolecular H-abstraction rate constant (k_{sq}), and the intercept is the sum of glyoxylate triplet decay and intramolecular H-abstraction rate constants ($k_d + k_{N_2}$).

SCHEME 2

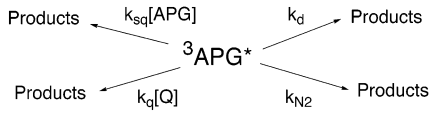

oxygen (Figure 13). This is consistent with the expected quenching of the glyoxylate triplet by oxygen and concommitance of the two kinetic profiles.

The possible reactions of APG triplet can be summarized in Scheme 2. In addition to the intra-(Norrish type II) and intermolecular (self-quenching) H-abstractions, the APG triplet undergoes nonchemical unimolecular decay and can interact with the quenchers such as oxygen or olefins.

Detailed kinetic information can be obtained from the present TR FTIR studies. In the absence of the quencher, the plot of k_{obs} vs [APG] yields a straight line, the slope of which is the intermolecular H-abstraction (self-quenching) rate constant (k_{sq}). The sum of intramolecular H-abstraction and the nonchemical triplet decay rate constants ($k_{N_2} + k_d$) is the intercept for the lines in Figure 14.

Using the approach outlined previously,[9,20] the rate of the nonchemical triplet decay can be determined using dilute solutions (0.1mM) of TBPG where contributions from all other

TABLE 1: Summary of Rate Constants Obtained for Alkyl Phenylglyoxylates (APGs) Using Time-Resolved FTIR Experiments

type of APG	$k_d \times 10^{-5}$, s^{-1}		$k_{N2} \times 10^{-6}$, s^{-1}				$k_{sq} \times 10^{-6}$, $M^{-1}\cdot s^{-1}$			
			hexane		benzene		hexane		benzene	
	hexane	benzene	decay	rise	decay	rise	decay	rise	decay	rise
MPG	1.4[a]	0.8[a]	1.2 (0.4)[b]	1.3 (0.4)[b]	1.4 (0.5)[b]	1.6 (0.5)[b]	59 (20)[b]	73 (24)[b]	11.2 (3.7)[b]	9.5 (3.2)[b]
EPG	1.4[a]	0.8[a]	2.7 (1.4)[b]	3.0 (1.5)[b]			69 (35)[b]	70 (35)[b]		
iPPG	1.4[a]	0.8[a]	3.4 (3.4)[b]	3.4 (3.4)[b]			38 (38)[b]	65 (65)[b]		

[a] Obtained using the UV LFP triplet nonchemical decay rates for TBPG where no γ-H-abstraction is possible. [b] Statistical factors of 3 (MPG), 2 (EPG), and 1 (iPPG) are included for numbers in the brackets, which represent the rate constants for intra- and intermolecular H-abstraction per single hydrogen atom.

processes are negligible. Conventional LFP was used to monitor the TBPG triplet transient absorption at 440 nm[9] and the nonchemical triplet decay rate constants (k_d) of 8.0×10^4 and 1.4×10^5 s^{-1} were obtained in benzene and hexane, respectively. Using the k_d values and the triplet lifetime of the corresponding glyoxylate in dilute solution (0.1−0.5 mM), the rate constant for the intramolecular H-abstraction (k_{N_2}) can be obtained and compared to the results obtained from the TR FTIR self-quenching experiments. The examination of the corresponding LFP kinetic profiles revealed k_{N_2} values as follows: 6.7×10^5 s^{-1}, MPG in benzene; 8.4×10^5 s^{-1}, MPG in hexane; 1.8×10^6 s^{-1}, EPG in hexane; 1.6×10^6 s^{-1}, iPPG in hexane. Previously,[9] the values of $k_{N_2} = 6.43 \times 10^5$ s^{-1} and $k_q = 2.0 \times 10^6$ $M^{-1}\cdot s^{-1}$ for MPG in benzene were reported.

Typical self-quenching plots obtained from the TR FTIR experiments are shown in Figure 14. The rate constants of intra- and intermolecular H-abstractions for MPG, EPG, and iPPG obtained from these plots are shown in Table 1. The values for k_{N_2} from Table 1 are slightly higher than the corresponding values obtained from LFP but the overall agreement is reasonable. The intramolecular H-abstraction rate constants in benzene and hexane for MPG are close indicating that these values could be the typical rate constants for the nonpolar medium and H-abstraction from hexane is too slow to compete with this process. The self-quenching rate constants (k_{sq}) for all examined glyoxylates are similar within the experimental uncertainty.

The absolute Norrish type II H-abstraction rate constants are larger by a factor of 2 for EPG and iPPG when compared to the corresponding MPG values. To completely understand the H-abstraction trends in various glyoxylates, statistical factors need to be taken into consideration by determining the H-abstraction rate constants per hydrogen atom for all three glyoxylates of interest. The numbers in brackets from Table 1 represent the H-abstraction rate constants per hydrogen atom. In the case of the intramolecular process, MPG has the smallest rate constant followed by EPG and iPPG. This is consistent with the structural differences in the MPG−EPG−iPPG series where hydrogen can be more easily abstracted from the tertiary γ-carbon of iPPG or from the secondary γ-carbon of EPG than from the primary γ -carbon of MPG owing to relative stability of corresponding biradicals.

In agreement with the previous studies of glyoxylates,[8−12] the k_{N_2} values are lower than the rate constants of intramolecular γ-hydrogen abstraction in simple phenyl ketones, which are reported to be in the 10^7-10^8 s^{-1} range.[21] This difference can be explained by ester group conformational issues in APGs presented using the molecular dynamics concept. Among many possible conformers existing in solution, cis- (*Z*) or trans- (*E*) conformations of the ester group would have the highest probability of existence with the *E*-conformer being more stable

SCHEME 3

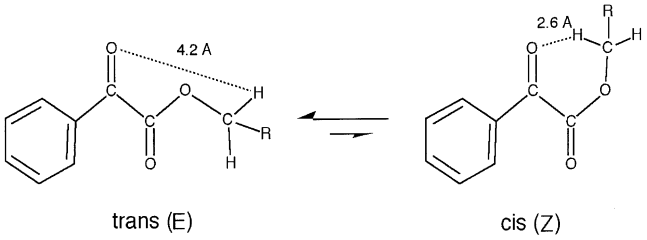

by 5−6 kcal/mol at room temperature.[22] DFT calculations indicate the *E*-conformer of MPG ground state is more stable by 5.2 kcal/mol (5.1 kcal/mol, corrected for the zero-point vibrational energy), which is consistent with the energy difference in other esters (5.4 kcal/mol, EPG, and 3.0 kcal/mol, iPPG). The smaller energy difference for iPPG can be explained by relative contributions of the steric effects introduced by the presence of two bulky methyl groups in both *Z*- and *E*-conformers. These energy differences indicate that probability of producing *Z*-conformer, which favors intramolecular H-abstraction, is smaller compared to the one for *E*-conformer (Scheme 3). Although ground-state geometry changes upon electronic excitation, one can assume that in n,π^* triplets of the aromatic carbonyl compounds, the ground state conformation serves as a reasonable representation of the excited state geometries because these changes are minor. It is known that electronic excitation only slightly lengthens the C═O bond[23] and makes the benzoyl group nearly coplanar.[24] In glyoxylates, γ-hydrogen abstraction by the keto-group is only possible when ester group is in the less probable *Z*-conformation. This is confirmed by the calculated (using DFT calculations) C═O⋯H−C distances for *E* and *Z* conformers of MPG. It is only 2.6 Å for *Z*-MPG and much longer (4.2 Å) for *E*-MPG. The former value is below the 3.0 Å threshold required for successful γ-hydrogen abstraction,[25] while the latter is far beyond the necessary limit. Thus, the small probability of generating the H-abstraction favorable *Z*-conformation from all noninteracting conformers in solution is responsible for more than 10-fold difference between the intramolecular H-abstraction rate constants of the aromatic ketones and glyoxylates.

Conclusions

Step-scan TR FTIR spectra of a series of alkyl phenylglyoxylates [10−40 mM] were obtained in hexane and benzene (MPG only). The results confirm the postulated intramolecular H-abstraction by direct observation of the time-resolved IR absorptions of glyoxylate triplet states around 1661 cm^{-1} and of the α-hydroxyphenyl ketene at 2105 cm^{-1}. Intra- and intermolecular H-abstraction rate constants determined from the TR IR data are found to be in agreement with the values

previously reported for MPG. The rate constants of intramolecular H-abstraction per single hydrogen atom decrease in the sequence iPPG > EPG > MPG, which is consistent with the relative order of the stability of the corresponding biradicals produced by the Norrish type II process. The conformational factors in glyoxylates are found to be responsible for the lower rate constants for intramolecular H-abstraction relative to the simple phenyl ketones.

Acknowledgment. The authors thank the National Science Foundation for financial support of this work (Grant DMR 9803006). Partial support from the U.S. Soybean Board is also acknowledged. We also thank Dr. Woojae Lee and Dr. Sergei Voskresensky for synthesis of iPPG and TBPG. We thank one of the reviewers for most insightful comments on this manuscript. A.G.M. is grateful to the McMaster Endowment for the fellowship.

References and Notes

(1) For example see: (a) Smith, J. D.; Maxwell, K. A.; DeSimone, J. M.; Meyer, T. J.; Palmer, R. A. *Inorg. Chem.* **2000**, *39*, 893−898. (b) Omberg, K. M.; Smith, G. D.; Kavaliunas, D. A.; Chen, P.; Treadway, J. A.; Schoonover, J. R.; Palmer, R. A.; Meyer, T. J. *Inorg. Chem.* **1999**, *38*, 951−956. (c) Chen, P.; Palmer, R. A.; Meyer, T. J. *J. Phys. Chem. A* **1998**, *102*, 3042−3047. (d) Chen, P.; Omberg, K. M.; Kavaliunas, D. A.; Treadway, J. A.; Palmer, R. A.; Meyer, T. J. *Inorg. Chem.* **1997**, *36*,954−955. (e) McFarlane, K.; Lee, B.; Bridgewater, J.; Ford, P. C. *J. Organomet. Chem.* **1998**, *554*, 49−61. (f) Schoonover, J. R.; Bingozzi, C. A.; Meyer, T. J. *Coord. Chem. Rev.* **1997**, *165*, 239−266. (g) Ford, P. C.; Bridgewater, J. S.; Lee, B. *Photochem. Photobiol.* **1997**, *65*, 57−64. (h) George, M. W.; Polyakov, M.; Turner, J. J. *Analyst* **1994**, *119*, 551−560.

(2) For example see: (a) Wang, J.; El-Sayed, M. *J. Phys. Chem. A* **2000**, *104*, 4333−4337. (b) Rodig, C.; Siebert, F. *FEBS Lett.* **1999**, *44*, 14−18. (c) Brudler, R.; Gerwert, K. *Photosynth. Res.* **1998**, *55*, 261−266. (d) Contzen, J. Jung, C. *Biochemistry* **1998**, *37*, *7*, 4317−4324. (e) Rammelsberg, R.; Hessling, B. Chorongiewski, H.; Gewert, K. *Appl. Spectrosc.* **1997**, *51*, 558−562. (f) Hu, X.; Frei, H. Spiro, T. G. *Biochemistry* **1996**, *35*, 13001−13005. (g) Hage, W.; Kim, M.; Frei H.; Mathies, R. A. *J. Phys. Chem.* **1996**, *100*, 16026−16033.

(3) For example, see: (a) Vasenkov, S.; Frei, H. *J. Phys. Chem. A* **2000**, *104*, 4327−4332. (b) Vasenkov, S.; Frei, H. *J. Phys. Chem. B* **1998**, *102*, 8177−8182. (c) Vasenkov, S.; Frei, H. *J. Am. Chem. Soc.* **1998**, *120*, 4031−4032. (d) Sun, H. Frei, H. *J. Phys. Chem. B* **1997**, *101*, 205−209. (e) Urano, T. I.; Hamaguchi, H. O. *Appl. Spectrosc.* **1993**, *47*, 2108−2113.

(4) For example, see: (a) Brown, C. E.; Neville, A. G.; Rayner, D. M.; Ingold, K. U.; Lusztyk, J. *Aust. J. Chem.* **1995**, *48*, 363−379. (b) Neville, A. G.; Brown, C. E.; Rayner, D. M.; Lusztyk, J.; Ingold, K. U. *J. Am. Chem. Soc.* **1991**, *113*, 1869−1870. (c) Neville, A. G.; Brown, C. E.; Rayner, D. M.; Lusztyk, J.; Ingold, K. U. *J. Am. Chem. Soc.* **1989**, *111*, 9269−9270. (d) Slugget, G. W.; Turro, C.; George, M. W.; Koptyug, I. V.; Turro, N. J. *J. Am. Chem. Soc.* **1995**, *117*, 5148.

(5) For example, see: (a) Moss, R. A.; Johnson, L. A.; Yan, S.; Toscano, J. P.; Showalter, B. M. *J. Am. Chem. Soc.* **2000**, *122*, 11256−11257. (b) Wang, Y. H.; Yuzawa, T.; Hamaguchi, H. O.; Toscano, J. P. *J. Am. Chem. Soc.* **1999**, *121*, 2875−2882. (c) Nigam, M.; Platz, M.; Showalter, B. M.; Toscano, J. P.; Johnson, R.; Abbot, S. C.; Kirchoooff, M. *J. Am. Chem. Soc.* **1998**, *120*, 8055−8059.

(6) For example, see: (a) Wang, Y.; Toscano, J. P. *J. Am. Chem. Soc.* **2000**, *122*, 4512−4513. (b) Srivastava, S.; Ruanne, P. H.; Toscano, J. P. Sullivan, M. B.; Cramer, C. J.; Chiapperino, D.; Reed, E. C.; Falvey, D. E. *J. Am. Chem. Soc.* **2000**, *122*, 8271−8278. (c) Wagner, B. D.; Arnold, B. R.; Brown, G. S.; Lusztyk. J. *J. Am. Chem. Soc.* **1998**, *120*, 0(8), 1827−1834. (d) Camara de Lucas, N.; Netto-Ferreira, J. C.; Andraos, J.; Lusztyk, J.; Wagner, B. D.; Scaiano, J. C. *Tetrahedron Lett.* **1997**, *38*, 5147−5150. (e) Allen, A. D.; Colomvacos, J. D.; Diederich, F.; Egle, I.; Hao, X.; Liu, R.; Lusztyk, J.; Ma, J.; McAllister, M.; Rubin, Y.; Sung, K.; Tidwell, T. T.; Wagner, B. D. *J. Am. Chem. Soc.* **1997**, *119*, 12125−12130. (f) Allen, A. D.; Colomvacos, J. D.; Egle, I.; Lusztyk, J.; McAllister, M.; Tidwell, T. T.; Wagner, B. D.; Zhoa, D. *J. Am. Chem. Soc.* **1995**, *117*, 7552−7553. (g) Wagner, B. D.; Zgierski, M. Z. Lusztyk. J. *J. Am. Chem. Soc.* **1994**, *116*, 6433−6434. (h) Arnold, B. R.; Brown, C. E.; Lusztyk, J. *J. Am. Chem. Soc.* **1993**, *115*, 1576−1577.

(7) Kauffmann, E.; Frei, H.; Mathies, R. A. *Chem Phys. Lett.* **1997**, *266*, 554−559. (b) Bucher, G.; Halupka, M.; Kolano, C.; Schade, O.; Sander, W. *Eur. J. Org. Chem.* **2001,** 545−552. (c) Cheng, Q.; Steinmetz, M. G.; Jayaraman, V. *J. Am. Chem. Soc.* **2002**, *124*, 7676−7677.

(8) Huyser, E. S.; Neckers, D. C. *J. Org. Chem.* **1964**, *29*, 276−78.

(9) Hu, S.; Neckers, D. C. *J. Org. Chem*. **1996**, *61*, 6407−6415.

(10) Encinas, M. V.; Lissi, E. A.; Zanocco, A.; Stewart, L. C.; Scaiano, J. C. *Can. J. Chem.* **1984**, *62*, 386-391.

(11) Hu, S.; Neckers, D. C. *J. Org. Chem.* **1997**, *62*, 755−757.

(12) Andraos, J.; Kresge, A. J. *Can. J. Chem.* **2000**, *78*, 508−515. (b) Chiang, Y.; Kresge, A. J.; Pruszynski, P.; Schepp, N. P.; Wirtz, J. *Angew. Chem., Int. Ed. Engl.* **1990**, *29*, 790−792.

(13) Fedorov, A. V.; Danilov, E. O.; Rodgers, M. A. J.; Neckers, D. C. *J. Am. Chem. Soc.* **2001**. In press.

(14) Hutson M. S.; Braiman, M. S. *Appl. Spectrosc*. **1998**, *52*, 974−984.

(15) Frisch, M. J.; Trucks, G. W.; Schlegel, H. B.; Scuseria, G. E.; Robb, M. A.; Cheeseman, J. R.; Zakrzewski, V. G.; Montgomery, J. A.; Stratmann, R. E.; Burant, J. C.; Dapprich, S.; Millam, J. M.; Daniels, A. D.; Kudin, K. N.; Strain, M. C.; Farkas, O.; Tomasi, J.; Barone, V.; Cossi, M.; Cammi, R.; Menucci, B.; Pomelli, C.; Adamo, C.; Clifford, S.; Ochterski, J.; Petersson, G. A.; Ayala, P. Y.; Cui, Q.; Morokuma, K.; Malick, D. K.; Rabuck, A. D.; Raghavachari, K.; Foresman, J. B.; Cioslowski, J.; Ortiz, J. V.; Baboul, A. G.; Stefanov, B. B.; G. Liu, A. L.; Piskorz, P.; Komaromi, I.; Gomperts, R.; Martin, R. L.; Fox, D. J.; Keith, T.; Al-Laham, M. A.; Peng, C. Y.; Nanayakkara, A.; Gonzales, C.; Challacombe, M.; Johnson, B.; Chen, W.; Wong, M. W.; Andres, J. L.; Head-Gordon, M.; Reprogle, E. S.; Pople, J. A. *Gaussian 98*, revision A.7; Gaussian Inc.: Pittsbugh, PA, 1998.

(16) Foresman, J. B.; Frisch, A. *Exploring Chemistry with Electronic Structure Methods*; Gaussian: Pittsburgh, PA, 1996.

(17) Lin-Vien, D.; Cothup, N. B.; Fatetey, W. G.; Graselli, J. G. *The Handbook of Infrared and Raman Characteristic Frequencies of Organic Molecules*; Academic: San Diego, CA, 1991.

(18) Tidwell, T. T. *Ketenes*; John Wiley and Sons: New York, 1995.

(19) Netto-Ferreira, J. C.; Scaiano, J. C. *Can. J. Chem.* **1993**, *71*, 1209−1215.

(20) Dalton, J. C.; Turro, N. J. *J. Am. Chem. Soc.* **1971**, *93*, 3569−3570.

(21) Wagner, P. J.; Park, B. In *Organic Photochemistry*; Padwa, A., Ed.; Marcel Dekker: New York, 1991; Vol. 11, pp 227−366.

(22) Eliel, E. L.; Wilen, S. H. *Stereochemistry of Organic Compounds*; Wiley: New York, 1994; pp 618−621.

(23) Chandler, W. D.; Goodman, L. *J. Mol. Spectrosc.* **1970**, *35*, 232−243. (b) Wagner, P. G. *Acc. Chem. Res.* **1983**, *16*, 461−467.

(24) Hoffmann, R.; Swenson, J. R. *J. Phys. Chem.* **1970**, *74*, 415−420.

(25) Scheffer, J. R.; Garcia-Garibay, M.; Nalamasu, O. *Org. Photochem.* **1987,** *8*, 249. (b) Ariel, S.; Ramamurthy, V.; Scheffer, J. R.; Trotter, J. *J. Am. Chem. Soc.* **1983**, *105*, 6959−6960. (c) Scheffer, J. R.; Dzakpasu, A. A. *J. Am. Chem. Soc.* **1978**, *100*, 2163-2173.